Nonparabolic effects in multiple quantum well structures and influence of external magnetic field on dipole matrix elements

Aleksandar Demić, Jelena Radovanović and Vitomir Milanović

***Abstract*—We present a method of modeling of nonparabolic effects (NPE) in quantum nanostructures by using second order perturbation theory. We apply this model on multiple quantum well structures and consider the influence of external magnetic field on dipole matrix element which is usually considered constant. The dipole matrix element directly influences the optical gain, and our model can provide a better insight to how NPE and magnetic field influence the gain of quantum nanostructures.**

***Index Terms*—Nonparabolicity effects; Quantum cascade lasers; Perturbation theory.**

Original Research Paper
DOI: 10.7251/ELS1519039D

I. Introduction

Nonparabolic effects (NPE) in the conduction band (CB) of a semiconductor quantum well (QW) material take an essential role in modeling the electronic structure of multiple QW structures such as quantum cascade laser (QCL). By using 14-band **kp** calculation presented in [1] Ekenberg in [2] determined the coefficients in the expansion of the dispersion relation up to the fourth order in wavevector. This results in a fourth order differential equation with boundary conditions obtained by double integration which fulfills the requirement for probability current conservation [3]. In [4] the authors presented the model from [2, 3] and its application on QCL structures by using the transfer matrix method (TMM).

QCL structures are powerful light sources emitting from mid-infrared (MIR) to THz frequencies, that turned out to be efficient and reliable in free-space communications, medical diagnostics, and chemical sensing [5-9].

Manuscript received 08 November 2015. Received in revised form 15 December 2015.

This work was supported by the Ministry of Education, Science and Technological development (Republic of Serbia), (Project III45010) and SfP Grant, ref. no. 984068.

Aleksandar Demić is with the School of Electrical Engineering, University of Belgrade, 73 Bulevar kralja Aleksandra, 11020 Belgrade, Serbia (e-mail: alexandardemic@yahoo.com).

Jelena Radovanović is with the School of Electrical Engineering, University of Belgrade, 73 Bulevar kralja Aleksandra, 11020 Belgrade, Serbia (e-mail: radovanovic@etf.bg.ac.rs).

Vitomir Milanović is with the School of Electrical Engineering, University of Belgrade, 73 Bulevar kralja Aleksandra, 11020 Belgrade, Serbia (e-mail: milanovic@etf.bg.ac.rs).

By engineering the active region, it is possible to obtain a wide range of operating wavelengths from 3 μm up to 250 μm. The lasing wavelength is defined by the separation of the laser energy state, and for THz frequencies the energy difference is very small (around 10meV) and thus any shift in energy can make modeling of these structures more demanding.

We will use the model from [2-4] and apply a second order perturbation theory in order to model energy corrections more accurately. We will also consider a first order correction for the wavefunction and this will allow us to study the effect of magnetic field on dipole matrix element, or in another sense the dependence of the gain of QCL. Nonparabolic effects are more pronounced in materials with smaller energy gaps due to a stronger mixing of the bands, thus we will also apply our model on structures with such properties.

II. Theoretical Consideration

The Hamiltonian presented in [2] in presence of magnetic field can be written as $\hat{H} = \hat{H}_{NP0} + \hat{H}_{NP}$, where $\hat{H}_{NP0}$ represents the part of the Hamiltonian $\hat{H}_{NP0} = \hat{H}\left(\hat{k}_{||} = 0\right)$ and it can be represented as the sum of the unperturbed Hamiltonian $\hat{H}_0 = \hat{k}_z^2\alpha_0(z)\hat{k}_z^2 + \frac{\hbar^2}{2}\hat{k}_z\frac{1}{m^*(z)}\hat{k}_z + V(z)$ and the perturbed Hamiltonian $\hat{H}' = \left(j_n + \frac{1}{2}\right)\frac{eB\hbar}{\hat{M}(z)}$. $\hat{H}_{NP}$ can be treated with the second order perturbation theory (first correction vanishes) and this was done in [2]. $\hat{H}_{NP}$ has the form $\left(2\alpha_0(z) + \beta 0z12kx,ky2+\alpha 0zkx4+ky4\right.$. The coefficients $\alpha 0$, $\beta 0$ are nonparabolic parameters, B is the magnetic induction of external magnetic field, $V\left(z\right)$ is the potential of the structure, $\hat{k}_x, \hat{k}_y, \hat{k}_z$ are the wavevector components operators, $m^*(z)$ is the effective mass at the bottom of conduction band and j_n is the Landau level index.

In this paper we focus on $\hat{H}_{NP0}$, and apply the second order perturbation theory. The Hamiltonian $\hat{H}$ oper-ates on the envelope wavefunction $\eta_n\left(z\right)$. We treat $\hat{H}_{NP0}$ and $\hat{H}_{NP}$ separately. For $\hat{H}_{NP0}$ we first solve the eigenvalue problem with non perturbated Hamiltonian $\hat{H}_0\eta_{n0}\left(z\right) = E_n^{(0)}\eta_{n0}\left(z\right)$ (index 0 depicts zeroth correction (unperturbed value), and indices $n=1,2,$ ... depict the bound state energy index) and use wavefunctions $\eta_{n0}(z)$ as the basis for perturbation theory with the perturbed Hamiltonian $\hat{H}'$. $\hat{H}_{NP}$ is treated with second

order perturbation theory in [2], first correction for energy $\Delta E_n^{(1)}$ is also determined in [2]. Corrections for energy are:

$$\begin{aligned}\Delta E_n^{(1)} &= \left(j_n+\frac{1}{2}\right)\frac{eB\hbar}{m^*_{||}}\\ \Delta E_n^{(2)} &= \left[\left(j_n+\frac{1}{2}\right)eB\hbar\right]^2\sum_{k\neq n}\frac{|M_{nk}|^2}{E_n^{(0)}-E_k^{(0)}}\\ \Delta E_{NP}^{(2)} &= [(8j_n^2+8j_n+5)<\alpha_0>+\\ &\quad (j_n^2+j_n+1)<\beta_0>]\frac{e^2B^2}{2\hbar^2}\end{aligned} \tag{1}$$

where $\frac{1}{m^*_{||}}=\int_{-\infty}^{\infty}\eta_{n0}^*\frac{1}{\widetilde{M}(z)}\eta_{n0}dz$ is parallel mass, $M_{nk}=\int_{-\infty}^{\infty}\eta_{n0}^*\frac{1}{\widetilde{M}(z)}\eta_{k0}dz$, $n\neq k$ are matrix elements of perturbed Hamiltonian and $<\alpha_0>$ and $<\beta_0>$ are the expected values of nonparabolic parameters.

The first order correction for envelope wavefunction is

$$\Delta\eta_n^{(1)} = e\hbar B\left(j_n+\frac{1}{2}\right)\sum_{k\neq n}\frac{M_{nk}}{E_n^{(0)}-E_k^{(0)}}\eta_{k0},\quad n\neq k. \tag{2}$$

Overall energy and envelope wavefunctions are given with $E=E_n^{(0)}+\Delta E_n^{(1)}+\Delta E_n^{(2)}+\Delta E_{NP}^{(2)}$ and $\eta_n=\eta_{n0}+\eta_n^{(1)}$.

The presence of external electric field introduces a linear z term in the potential $V(z)$ of unperturbed Hamiltonian which results in continuous energy spectrum. In the case of moderate external electric fields, the energy states that were previously bound evolve into the so-called quasi-bound states after the application of bias, and they can then still be treated as bound under the additional assumption that the potential is constant far enough from the well [10]. These quasi-bound states can be determined by numerical solving of the $\widehat{H}_0$ eigen value problem and then energy and wavefunction corrections can be calculated.

The application of the perturbation theory is limited by the condition $|H'_{nk}|\ll E_n^{(0)}-E_k^{(0)}$. The perturbed Hamiltonian depends on magnetic induction and Landau level index and this condition imposes constraints on the values of these parameters. The second condition which limits our model emerges from the dispersion relation in bulk material, as presented in [4]. By solving the quantum well structure we can easily determine dispersion relation in the form $E(k)=\alpha_0k^4+\frac{\hbar^2}{2m^*}k^2$ which has a maximum value of $E_{max}=\left(16m^{*2}/\hbar^4|\alpha_0|\right)^{-1}\approx 3.63|\alpha_0|^{-1}m'^{-2}$ [eV] where $m^*=m'\,m_0$ and α_0 is inserted in [eVÅ^4]. The authors in [4] noted that the model is applicable up to the turning point of the dispersion relation, but we claim its applicability up to E_{max}. The conditions for the application of our model are:

$$\begin{aligned}&B\left(j+\frac{1}{2}\right)\ll P_t,\qquad P_t=\min\left(\frac{\left|E_n^{(0)}-E_k^{(0)}\right|}{e\hbar|M_{nk}|}\right),\\ &\qquad n\neq k\\ &E<E_{max},\qquad E_{max}\approx\frac{3.63}{|\alpha_0|m'^2}\text{ [eV]}.\end{aligned} \tag{3}$$

We will consider the first condition in (3) satisfied for $B\left(j+\frac{1}{2}\right)\leq 0.1\,P_t$. The parameter P_t mostly depends on the energy separations and we expect that it will cause rigorous constraint for magnetic fields in terahertz QCL structures. The second condition benefits from low effective masses in III-V semiconductors, but deteriorates for large values of the nonparabolic parameter α_0. In most cases of interest E_{max} will be lower than the conduction band offset and it will not be possible to consider all states in the structure. Our greatest interest is usually in the lower states of considered QW or QCL, hence if E_{max} is greater than all the states of interest, we will continue with the application of the model. This approximation is possible due to the fact that in perturbation theory higher states have lesser effect on the lower states when calculating corrections in (1) and (2).

Equations (1)-(3) represent a complete model of the second order perturbation theory of NPE in semiconductor nanostructures.

Since we included first order correction for wavefunction we can discuss its effect on the dipole transition element. The dipole transition matrix element is defined as $d_{if}=\int_{-\infty}^{\infty}\eta_i^*\,z\,\eta_f dz$ where index i refers to an initial state, and f to a final state of the optical transition. The envelope wavefunctions η_i, η_f are usually chosen as unperturbed wavefunctions, but by including correction we will be able to analyze the influence of magnetic field on the properties of our structure. Inserting (2) in d_{if} yields:

$$\begin{aligned}d_{if} &= d_{if}(0)\\ &+B\left(j+\frac{1}{2}\right)\left[\int_{-\infty}^{\infty}\left(\eta_i^{(1)^*}z\,\eta_{f0}+\eta_{i0}^*\,z\,\eta_f^{(1)}\right)dz\right]\\ &\quad+B^2\left(j+\frac{1}{2}\right)^2\int_{-\infty}^{\infty}\eta_i^{(1)^*}\,z\,\eta_f^{(1)}dz\end{aligned} \tag{4}$$

where $d_{if}(0)=\int_{-\infty}^{\infty}\eta_{i0}^*\,z\,\eta_{f0}dz$. The third term in (4) is very small and we can assume that the behavior of d_{if} is linear with magnetic field in most cases. Note that first order corrections for the envelope wavefunctions are linearly proportional to the non-parabolic parameters α_0 and β_0 (because of the matrix elements of perturbed Hamiltonian M_{nk} in eq. (1)), hence we expect greater rates of change in materials with great nonparabolicity but on the other hand the conditions in (3) will also become more rigorous. Modeling of these parameters and their determination in III-V semiconductor and alloys of interest are given in [11].

The importance of the dipole matrix element lies in the fact that gain and absorption values of optical transitions depend on $\left|d_{if}\right|^2$. Let us consider a 3-states QCL structure $E_1<E_2<$

E_3 with two transitions of interest: $E_3 \rightarrow E_2$ (lasing transition) and $E_2 \rightarrow E_1$ (transition for depopulation of the second state). Most models of QCL structures calculate the dipole matrix element in (4) with unperturbed wavefunctions (only first term in (4)), thus the effect of external magnetic field cannot be seen. In this paper we will illustrate the dependence of the dipole matrix element on B for different Landau levels by using wavefunctions with first order correction.. Also (3) gives us the values of magnetic field B_j which limit the application of the perturbation theory. As mentioned in [12], in the presence of external magnetic field the optical gain which corresponds to transitions $(3,j)\rightarrow(2,j)$ depends on $E_{3,j} - E_{2,j}$. The authors in [12] included first order corrections for the energy, the model presented in this paper includes higher correction. The optical gain of this transition now has the form:

$$g_{3\rightarrow 2}(B) = \frac{2e^2\pi}{\bar{n}\varepsilon_0\lambda}\sum_j \left|d_{3,2,j}(B)\right|^2 \times \delta\left(E_{3,j}(B) - E_{2,j}(B) - \hbar\omega\right)\left(N_{3,j}(B) - N_{2,j}(B)\right)$$

$$E_{3,j} - E_{2,j} = E_3^{(0)} - E_2^{(0)} + e\hbar B\left(j+\frac{1}{2}\right)\left(\frac{1}{m_{||3}} - \frac{1}{m_{||2}}\right) + \left(\left(j+\frac{1}{2}\right)e\hbar B\right)^2 \times \left(\sum_{k\neq 3}\frac{|M_{3k}|^2}{E_3^{(0)} - E_k^{(0)}} - \sum_{k\neq 2}\frac{|M_{2k}|^2}{E_2^{(0)} - E_k^{(0)}}\right) + [(8j^2+8j+5)\Delta<\alpha_0> + (j^2+j+1)\Delta<\beta_0>]\frac{e^2B^2}{2\hbar^2} \quad (5)$$

where $\bar{n}$ is the material refractive index, λ and ω denote the wavelength and the frequency of the emitted light, $N_{3,j} - N_{2,j}$ represents the degree of population inversion, while $\Delta<\alpha_0>$ and $\Delta<\beta_0>$ represent differences of expectation values when wavefunctions of third and second states are used. The greatest addition to the gain in (5) arrives from the states with lower values of Landau level index. In numerical approach Dirac delta function can be substituted with suitable Lorentzian as explained in [12].

III. Numerical Results

Applying our model to structures in presence of electric field demands numerical solving of equations (1)-(4). We assume that moderate electric field is applied and that we can approximate the potential at the structure ends to be constant [10]. We use TMM method to determine energies and wavefunctions of Hamiltonian $\hat{H}_0$. These quasi-bound states are then used in perturbation theory.

We will apply our model on three QCL structures which will illustrate behavior of dipole matrix elements. Firstly we focus on the structure presented in [12] which is optimized for $\lambda = 10$ μm and has the following layer widths 25, **30**, 59, **12**, 59 Å (bold are $Al_{0.4}Ga_{0.6}As$ barriers and in normal text are GaAs wells) with a barrier height of 330 meV. The applied electric field is $K = 35.81\ kVcm^{-1}$. The potential of the structure and the corresponding envelope wavefunctions are presented in Fig. 1.

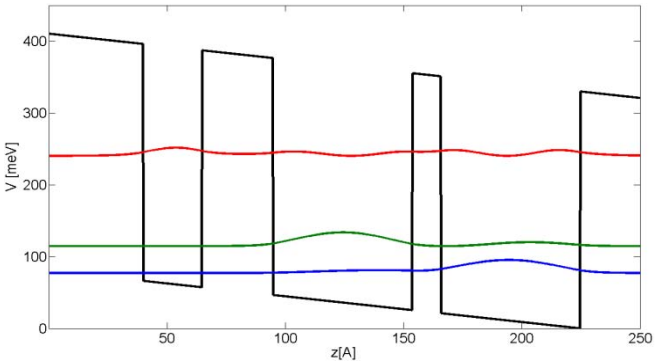

Fig. 1. The active region of QCL [12] under an electric field of $K = 35.81\ kVcm^{-1}$ and magnetic field of incduction $B = 0\ T$. Relevant energies and the moduli squared of non-perturbated wavefunctions are also displayed.

Energy levels in Fig. 1 are E_1=77.1 meV, E_2=114.5 meV and E_3=240.3 meV which corresponds to a lasing wavelength of $\lambda \approx 9.85\ \mu m$, which is in good correspondence with [12]. Under the influence of an external magnetic field we can calculate corrections for energy and wavelength by using our model. The conditions in (3) give $E_{max} = 384$ meV for GaAs and limiting magnetic fields are B_0=234.7 T, B_1=78.2 T, B_2=46.9 T, B_3=33.5 T, B_4=23 T, B_5=21.3 T, due to physical relevance we are interested in results below 60 T. In (5), optical gain depends on $E_{3,j} - E_{2,j}$ and $\left|d_{3,2,j}(B)\right|^2$, authors in [12] considered first order corrections for energy, difference $E_{3,j} - E_{2,j}$ with second order corrections is presented in Fig. 2 and $\left|d_{3,2,j}(B)\right|^2$ is presented in Fig 3.

Figure 2 shows how lasing energy difference depends on magnetic field. We can see that for constant magnetic field this difference decreases when higher Landau levels are considered. The lasing wavelength is defined by $E_{3,0} - E_{2,0}$ and in Fig 2. we can see that this value slightly varies with magnetic field which opens possibilities of tuning.

Figure 3 shows how square moduli of the dipole matrix element depends on magnetic field for lasing transition. For higher Landau levels we have more a pronounced decrease of $|d_{32}|^2$ than for lower ones. Lower Landau levels give the greatest contribution to the gain in (5), the authors in [12] estimated that the highest gain is achievable around 45-50 T without taking into account variation of $|d_{32}|^2$ with magnetic field. The results in Fig. 3 show that optical gain would be lower approximately 1-5 % (assuming that $j = 0,1$ are the dominant terms in (5) and that second order corrections for the energy in $E_{3,j} - E_{2,j}$ do not contribute significantly).

We can also calculate $|d_{21}|^2$ which is responsible for depopulation of the second state. Note that for $|d_{21}|^2$ Landau levels of both states can be arbitrary, thus we will separately present radiative transitions $j_1 = j_2 = j$ (Figure 4) and non-radiative transitions $j_1 \neq j_2$ (Figure 5).

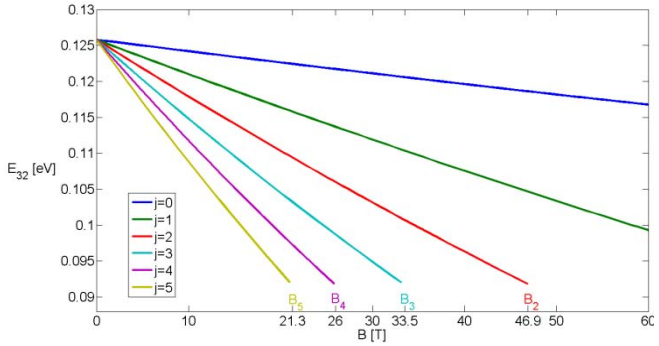

Fig. 2. Lasing energy difference for structure from [12] depending on magnetic induction for different Landau levels.

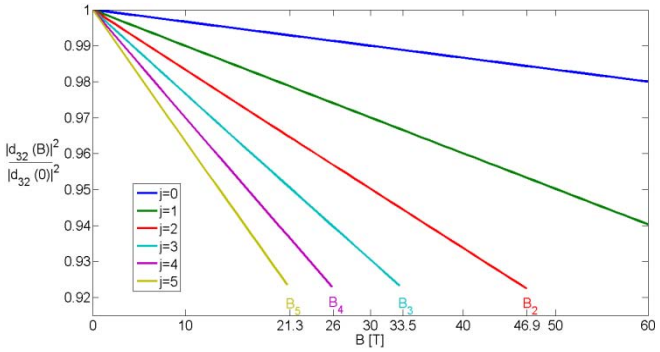

Fig. 3. Dipole matrix element $|d_{32}|^2$ for structure from [12] depending on magnetic induction for different Landau levels and $|d_{32}(0)| = 21.2$ Å.

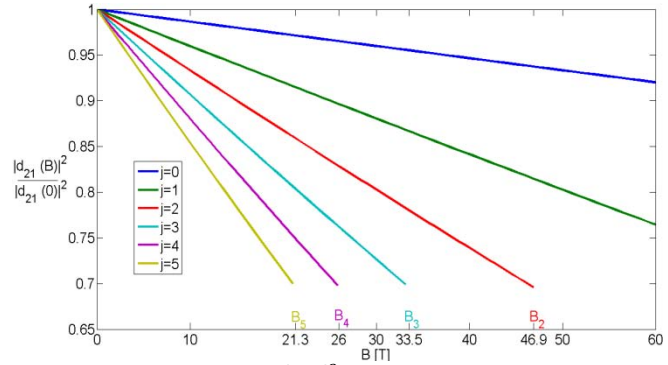

Fig. 4. Dipole matrix element $|d_{21}|^2$ for structure from [12] depending on magnetic induction for different Landau levels (and $j_1 = j_2 = j$) and $|d_{21}(0)| = 27.4$ Å.

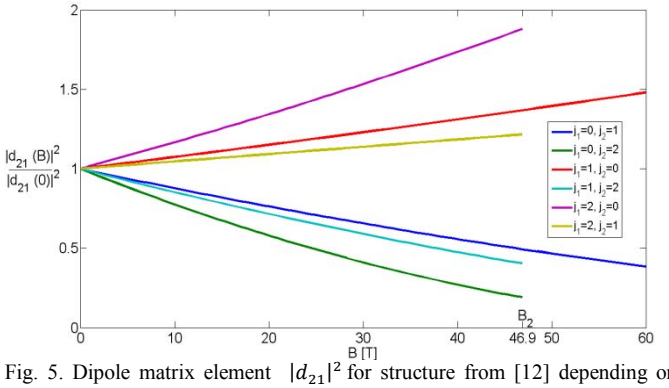

Fig. 5. Dipole matrix element $|d_{21}|^2$ for structure from [12] depending on magnetic induction for different Landau levels (and $j_1 \neq j_2$).

Figure 4 shows how square moduli od dipole matrix element depends on magnetic field for optical transition $2 \rightarrow 1$ when both states have same value of Landau level. The effect is more pronounced than the transition $3 \rightarrow 2$ (fig. 3) and we have an extensive decrease of dipole matrix element.

Figure 5 shows $|d_{21}|^2$ when Landau levels for particular states do not match. We can see that for $j_1 < j_2$ we have a decrease of the dipole matrix element while for $j_1 > j_2$this does not occur. The effect is even more extensive than in previous transitions and for certain values of magnetic field and Landau level indices we nearly have a minimal value.

In this example we see that the dipole matrix element mostly decrease with magnetic field, and that the decrease is stronger for higher Landau levels.

Next we consider the structure realized in [13] for emission at $\lambda \approx 68$ μm (and designed for 66 μm). The active region layer widths are 82, **17**, 68, **40**, 164, **34**, 90 Å (GaAs wells are in normal text, $Al_{0.15}Ga_{0.85}As$ are in bold text) with a barrier height of 125.5 meV. Applied electric field is 10.2 $kV\ cm^{-1}$. The potential of the structure and the unperturbed wavefunctions are shown in Fig 6.

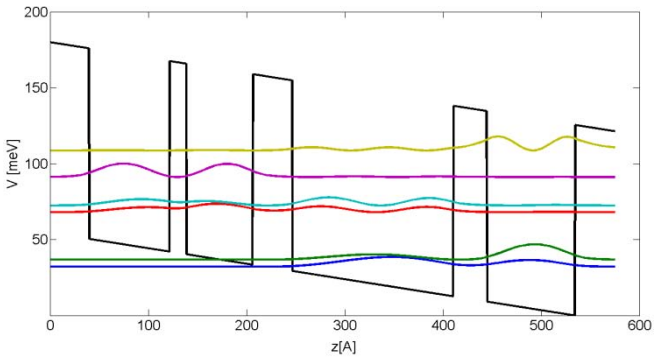

Fig. 6. The active region of QCL [13] under an electric field of $K = 10.2\ kVcm^{-1}$ and magnetic field induction$B = 0\ T$. Relevant energies and the moduli squared of non-perturbated wavefunctions are also displayed.

The states of interest in Fig. 6 are E_2=36.73 meV, E_3=67.97 meV, E_4=72.38 meV and E_5=91.11 meV. Lasing transition occurs between $5 \rightarrow 4$ or $5 \rightarrow 3$, which corresponds to a difference of E_{54}=18.73 meV and a lasing wavelength of $\lambda_{54} \approx 66.2$ μm, which is in good correspondence with the results from [13]. The maximum energy from condition (3) is 384 meV and this condition does not add limits to our model, but the perturbation theory condition does. Limiting magnetic fields are B_0=2.1 T, B_1=2.5 T, B_2=3.3 T, B_3=4.6 T, B_4=7.7 T, B_5=23.2 T. With unperturbed wavefunctions from Fig. 6 we can calculate energy and wavefunction corrections, lasing difference E_{54} is given in Fig. 7, while results for dipole matrix element for lasing transition is given in Fig. 8.

In Fig. 7 we can see that the energy difference of transition $5 \rightarrow 4$ varies linearly with magnetic field which means that second order corrections are very small. In Figure 8 we can see a mild change of dipole matrix element with magnetic field. It is interesting that in this example we have an increasing effect. Our simulations show that the dipole matrix element for optical transition $3 \rightarrow 2$ used for resonant depletion also increases with magnetic field for both radiative and non- radiative transitions more extensively (up to 15%). This example illustrates that the dipole matrix element can also rise with magnetic field.

The considered material of QW in the previous two examples was GaAs which has low nonparabolicity parameters due to a large energy gap. Both examples showed mild changes of the dipole matrix element for lasing transition. The model in [11] shows that low gap materials would give much higher nonparabolicity. On the other hand, the maximum energy condition in (3) becomes more rigorous and we are unable to model QCL structures made from InAs which would give nearly 30 times higher nonparabolicity parameters than GaAs. Fortunately we are able to model structures designed for terahertz applications because in most cases the energy states of interest are sufficiently below the maximum energy and we can consider low gap materials such as GaSb which has roughly 4 times higher parameters than GaAs. structures for terahertz range have narrow energy separations and modeling NPE is highly important. At the same time, the narrow energy separation will also cause perturbation theory condition in (3) to be much more rigorous.

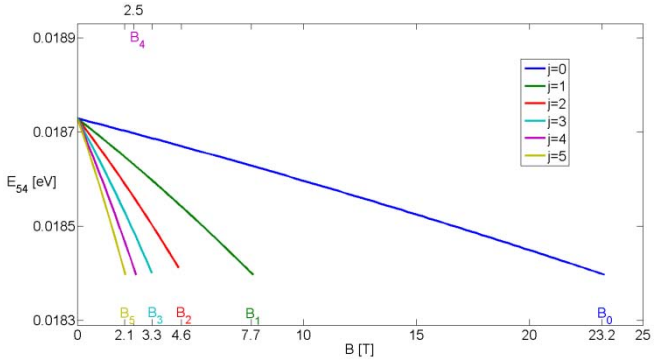

Fig. 7. Lasing energy difference for structure from [13] depending on magnetic induction for different Landau levels.

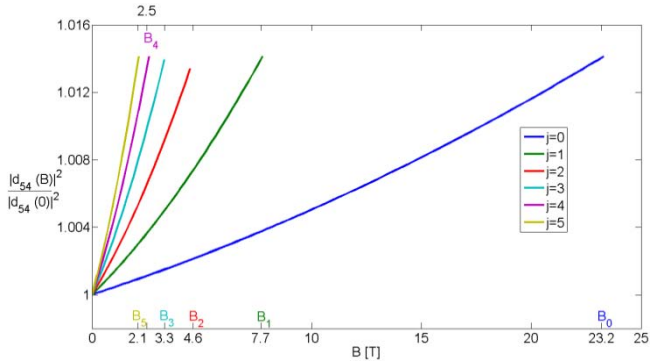

Fig. 8. Dipole matrix element squared, $|d_{54}|^2$ for the structure from [13] as a function of magnetic induction for different Landau levels and $|d_{54}(0)| = 56.6$ Å.

We will consider a terahertz QCL proposed and experimentally realized in [14] for lasing at $\lambda \approx 115.3$ μm (2.6 THz) and $\lambda \approx 157.9$ μm (1.9 THz) which corresponds to transitions E_{53}=10.6 meV and E_{54}=7.7 meV, respectively, with a phonon longitudinal energy of E_{32}=28.9 meV. This is a 4-well structure with the layer widths of active region 144, **24**, 114, **38**, 246, **30**, 162 Å (bold AlSb barriers and non-bold are GaSb wells) with barrier height of 1090 meV. Applied electric field is 5.4 $kV\,cm^{-1}$. The maximum energy from condition (3) is $E_{max} \approx 201$ meV, nonparabolicity parameters in GaSb are $\alpha_0 = -10730$ eV Å^4, $\beta_0 = -11473$ eV Å^4 and in the AlSb are $\alpha_0 = -330$ eV Å^4, $\beta_0 = -2342$ eV Å^4. The solutions of unperturbed Hamiltonian are shown in Fig. 9.

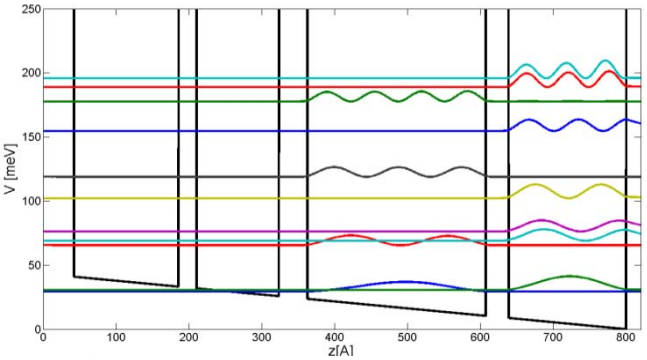

Fig. 9. The active region of QCL [14] under an electric field of $K = 5.4\ kVcm^{-1}$ and magnetic field of incduction $B = 0\ T$. Relevant energies and the moduli squared of non-perturbated wavefunctions are also displayed. Barrier height is 1090 meV, the picture is zoomed for better view.

The barrier height is 1090 meV and condition in (3) gives maximum energy of 201 meV, but energies of interest are below 80 meV and our model is applicable under the assumption that higher states do not contribute greatly to perturbation theory corrections. In Fig. 9 we can see that 11 states can be modeled. The states of interest are E_1=29.36 meV, E_2=30.5 meV, E_3=65.46 meV, E_4=68.96 meV and E_5=76.22 meV. Lasing transition occurs between $5 \rightarrow 4$ or $5 \rightarrow 3$, which correspond to differences of E_{54}=7.24 meV and E_{53}=10.76 meV and wavelengths $\lambda_{54} \approx 170.5$ μm (1.7 THz), $\lambda_{53} \approx 115.2$ μm (2.6 THz) respectively, which is in good correspondence with the results from [14].

Conditions (3) yield B_0=0.75 T, B_1=0.25 T, B_2=0.15 T, B_3=0.1 T, B_4=0.08 T, B_5=0.07 T, above these values theory of perturbation is not applicable (for the corresponding Landau level). The reason for this is a narrow energy seperation and also the fact that P_t depends on M_{nk} (in eq. (1)), which depends on magnetic field and nonparabolic parameters. The energy difference E_{54} is given in Fig. 10, while the results for the dipole matrix element for transition $5 \rightarrow 4$ are given in Fig. 11

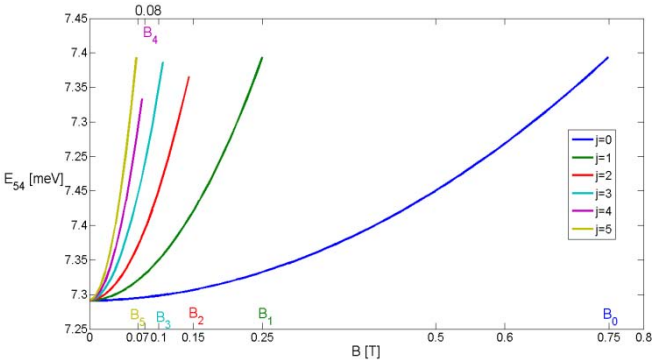

Fig. 10. Lasing energy difference for structure from [14] depending on magnetic induction for different Landau levels.

In Fig. 10 we can see that the energy difference of transition $5 \rightarrow 4$ clearly has a square dependence on magnetic field which shows the importance of including the second order corrections from (1). Fig. 10 also indicates that possible tuning

is also not linear with magnetic field. In Figure 11 we can see an extensive decrease of the dipole matrix element for low magnetic field. If the condition in (3) were less rigorous these curves would reach minimal value below magnetic field of 1T. In eq. (4) we can see that the dipole matrix element has a second order polynomial dependence on B, and after the minimal value we would expect a rise of curves in Fig. 11 if the perturbation theory condition were less rigorous. This example illustrates the importance of modeling the dipole matrix element when an external magnetic field is applied. The results in Fig. 11 indicate that the dipole matrix element will deteriorate up to 8% for magnetic fields under 1T.

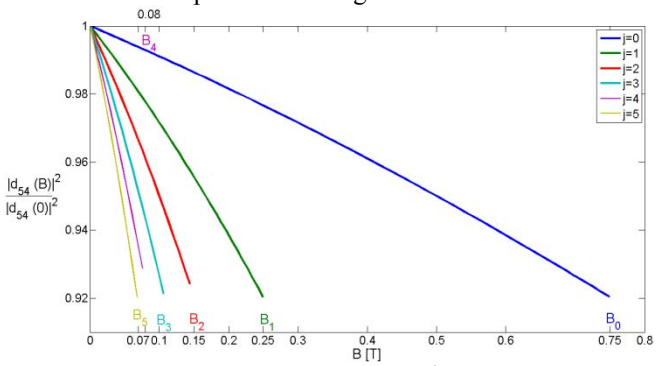

Fig. 10. Dipole matrix element squared, $|d_{54}|^2$ for the structure from [14] as a function of magnetic induction for different Landau levels and $|d_{54}(0)| = 711.3$ Å.

In this example the dipole matrix element for optical transition $3 \rightarrow 2$ used for resonant depletion decreases with magnetic field for both radiative and non-radiative transitions more extensively.

IV. Conclusion

In [4] the authors showed that TMM method in combination with NPE can be applied to various QCL structures. In this paper we generalized that model and presented how magnetic field influences QCL structures.

We presented effects of magnetic field on the dipole matrix element by using a 2nd order perturbation theory with Hamiltonian which includes NPE. We formed a model (1)-(3) which also includes a 1st order correction for envelope wavefunction and 2nd order corrections for energy. The application of the model is limited by the perturbation theory condition and the condition which arises from the dispersion relation of the considered Hamiltonian. Applied to a QCL structure, this model gives us new insights on.

We showed that the dipole matrix element changes its values with different speed rates with Landau level and that in some cases the effects of external magnetic field on the dipole matrix element can not be neglected, especially in structures with high nonparabolicity (lower energy gap of quantum well material).

References

[1] M. Braun, U. Rossler, "Magneto-optic transitions and non-parabolicity parameters in the conduction band of semiconductors" *J. Phys. C: Solid State Phys.* 18, 3365-3379, 1985.

[2] U. Ekenberg, "Nonparabolicity effects in a quantum well: Sublevel shift, parallel mass, and Landau levels" *Phys. Rev. B* 40 7714-7726, 1989.

[3] V. Milanović, J. Radovanović, S. Ramović, "Influence of nonparabolicity on boundary conditions in semiconductor quantum wells" *Phys. Lett. A* 373, 3071-3074, 2009.

[4] N. Vuković, J. Radovanović., V. Milanović, "Enhanced modeling of band nonparabolicity with application to a mid-IR quantum cascade laser structure" *Physica Sripta* T162**,** 014014, 2014.

[5] C. Gmachl, F. Capasso, D. Sivco, A. Cho, "Recent progress in quantum cascade lasers and applications" *Rep. Prog. Phys.* 64 1533, 2001.

[6] J. Faist, F. Capasso , D. Sivco, C. Sirtori, A. Hutchinson, A. Cho, "Quantum Cascade Laser" *Science* 264 553-556, 1994.

[7] A. Kosterev, F. Tittel, "Chemical Sensors Based on Quantum Cascade Lasers" *IEEE J. Quantum Electron.* 38 582-591, 2002.

[8] G. Wysocki, R. Lewicki., R. Curl, F. Tittel, L. Diehl, F. Capasso, M. Troccoli, G. Hofler, D. Bour, S. Corzine, R. Mualini, M. Giovannini , J. Faist, "Widely tunable mode-hop free external cavity quantum cascade lasers for high resolution spectroscopy and chemical sensing". *Appl. Phys.B* 92 305-311, 2008.

[9] J. McManus, J. Shorter, D.Nelson, M. Zahnister, D. Glenn, R. McGovern, " Pulsed quantum cascade laser instrument with compact design for rapid, high sensitivity measurements of trace gases in air" *Appl. Phys.B* 92 387-392, 2008.

[10] Z. Ikonić, V. Milanović, *Semiconductor Quantum Microstructures*, Belgrade, Republic of Serbia, University of Belgrade, 1997.

[11] V. Golubev, V. Ivanov-Omskii, I. Minervin, A. Osutin, D. Polyakov ''Nonparabolicity and anisotropy of the electron energy spectrum in GaAs'' *Zh. Eksp. Teor. Fiz*. 88, 2052-2062, 1985. [Sov. Phys. JETP 61, 1214 (1985)].

[12] J. Smiljanić, M. Žeželj, V. Milanović, J. Radovanović, I. Stanković, "MATLAB-based program for optimization of quantum cascade laser active region parameters and calculation of output characteristics in magnetic field" *Comput. Phys Commun.185*, 998-1006, 2014.

[13] B. Williams, S. Kumar, Q. Hu, J. Reno, "High-power terahertz quantum-cascade lasers" *Electron. Lett. 42,* 20063921, 2006.

[14] H. Yasuda, I. Hosako, S. Miyashita, M. Patrashin ''Terahertz electroluminescence from GaSb=AlSb quantum cascade laser'' *Electronics Letters vol.41, no.19*, 1062-1063, 2005.